



The $v_3^{1/3}/v_2^{1/2}$ ratio in PbAu collisions at $\sqrt{s_{NN}} = 17.3$ GeV: a hint of a hydrodynamic behavior

CERES/NA45 Collaboration

D. Adamová¹, G. Agakishiev², A. Andronic³, D. Antończyk⁴, H. Appelshäuser⁴, V. Belaga^{†2}, J. Bielčíková^{5,6,7}, P. Braun-Munzinger⁸, O. Busch^{†9}, A. Cherlin¹⁰, S. Damjanović⁹, T. Dietel³, L. Dietrich⁹, A. Drees¹¹, W. Dubitzky⁹, S. I. Esumi^{9,12}, K. Filimonov^{9,13}, K. Fomenko², Z. Fraenkel^{†10}, C. Garabatos⁸, P. Glässel⁹, G. Hering⁸, J. Holeczek⁸, M. Kalisky³, G. Krobath⁹, V. Kushpil¹, A. Maas⁸, A. Marín⁸, J. Milošević^{9,14,15,a}, D. Miśkowiec⁸, Y. Panebrattsev², Z. Paulínová¹⁶, O. Petchenova², V. Petráček^{7,9}, S. Radomski⁹, J. Rak⁵, I. Ravinovich¹⁰, P. Rehak^{†17}, H. Sako⁸, W. Schmitz⁹, S. Schuchmann⁴, S. Sedykh⁸, S. Shimansky², J. Stachel⁹, M. Šumbera¹, H. Tilsner⁹, I. Tserruya¹⁰, G. Tsileadakis⁸, J. P. Wessels³, T. Wienold⁹, J. P. Wurm^{†5}, S. Yurevich^{2,9}, V. Yurevich²

- ¹ Nuclear Physics Institute, Czech Academy of Sciences, 25068 Řež, Czech Republic
² Joint Institute of Nuclear Research, Dubna 141980, Moscow Region, Russia
³ Institut für Kernphysik, Universität Münster, 48149 Münster, Germany
⁴ Institut für Kernphysik, Johann Wolfgang Goethe-Universität Frankfurt, 60438 Frankfurt, Germany
⁵ Max-Planck-Institut für Kernphysik, 69117 Heidelberg, Germany
⁶ Present Address: Nuclear Physics Institute, Czech Academy of Sciences, 25068 Řež, Czech Republic
⁷ Present Address: Czech Technical University in Prague, Faculty of Nuclear Sciences and Physical Engineering, 11519 Prague, Czech Republic
⁸ Research Division and Extreme Matter Institute (EMMI), GSI Helmholtzzentrum für Schwerionenforschung, 64291 Darmstadt, Germany
⁹ Physikalisches Institut, Universität Heidelberg, 69120 Heidelberg, Germany
¹⁰ Department of Particle Physics, Weizmann Institute, Rehovot 76100, Israel
¹¹ Department for Physics and Astronomy, SUNY Stony Brook, Stony Brook, NY 11974, USA
¹² Present Address: Institute of Physics, University of Tsukuba, Tsukuba, Japan
¹³ Present Address: Physics Department, University of California, Berkeley, CA 94720-7300, USA
¹⁴ Present Address: “VINČA” Institute of Nuclear Science-National Institute of the Republic of Serbia, University of Belgrade, Mike Petrovića Alasa 12-14, Vinča, Belgrade 11351, Serbia
¹⁵ Also at: Strong-coupling Physics International Research Laboratory, Huzhou University, Huzhou, China
¹⁶ Faculty of Science, P. J. Šafárik University, Kosice, Slovakia
¹⁷ Instrumentation Division, Brookhaven National Laboratory, Upton, NY 11973-5000, USA

Received: 6 June 2024 / Accepted: 25 September 2024
© The Author(s) 2024

Abstract The Fourier harmonics, v_2 and v_3 of negative pions are measured at center-of-mass energy per nucleon pair of $\sqrt{s_{NN}} = 17.3$ GeV around midrapidity by the CERES/NA45 experiment at the CERN SPS in 0–30% central PbAu collisions with a mean centrality of 5.5%. The analysis is performed in two centrality bins as a function of the transverse momentum p_T from 0.05 GeV/ c to more than 2 GeV/ c . This is the first measurement of the $v_3^{1/3}/v_2^{1/2}$ ratio as a function of transverse momentum at SPS energies, that reveals, independently of the hydrodynamic models, hydrodynamic behavior of the formed system. For p_T above 0.5 GeV/ c , the ratio is nearly flat in accordance with the hydrodynamic prediction and as previously

observed by the ATLAS and ALICE experiments at the much higher LHC energies. The results are also compared with the SMASH-vHLLÉ hybrid model predictions, as well as with the SMASH model applied alone.

1 Introduction

At sufficiently high energy density as achieved in ultra-relativistic heavy-ion collisions, a dense and hot system of strongly coupled quarks and gluons called quark-gluon plasma (QGP) is created [1–7]. Anisotropic pressure gradients, built early in the collision, cause a collective azimuthally anisotropic expansion of the QGP that converts initial spatial anisotropy into a momentum anisotropy that was observed

^a e-mail: Jovan.Milosevic@cern.ch

first at the BNL AGS (E877) [8], then at the CERN SPS (NA49, WA98, CERES) [9–11] and finally at Relativistic Heavy Ion Collider (RHIC) and Large Hadron Collider (LHC) experiments [12–22]. This azimuthal anisotropy of particles emitted in the final state can be used to explore the hydrodynamic behavior of the hot and dense systems created in such collisions. The almond-like shape of the overlapping region in a non-central nucleus-nucleus collision causes the appearance of the elliptic flow (v_2) anisotropy [23]. Moreover, the positions of nucleons in the colliding nuclei fluctuate. These event-by-event fluctuations have a significant influence on the QGP expansion [24] and cause the appearance of higher-order anisotropies. The most pronounced is the triangular flow (v_3) that is measured at both RHIC [25–29] and the LHC [13, 17, 21, 22] in central and non-central collisions.

At the high collision energies achieved at RHIC and LHC, large v_2 values are observed that agree well with predictions of relativistic hydrodynamics [30] without dissipation, suggesting that elliptic flow is built early in the evolution of the QGP, and that the QGP behaves as a nearly perfect liquid, see the reviews in [31, 32]. The measured v_2 is also well described with a hybrid calculation that treats the QGP by ideal hydrodynamics [23] and the late stages of the collision by a hadronic cascade model [33]. The description can be refined by taking viscosity into account [34, 35]. The viscosity makes the v_2 magnitudes somewhat smaller with respect to the ideal hydrodynamic limit. The viscous hydrodynamic models like MUSIC [36, 37] and VISHNU [38] have been developed to describe azimuthal anisotropies. A very good agreement between the IP Glasma+MUSIC [39], as well as the VISHNU model predictions [40], and the experimentally measured azimuthal anisotropies at RHIC and LHC are obtained. Relativistic hydrodynamic models achieved to give semiquantitative constraints on specific viscosity (η/s), but with large uncertainties. Comprehensive model-data analyses that use a Bayesian approach allow a temperature-dependent specific viscosity [41]. The obtained values of η/s , depending on the temperature, vary from 0.1 up to 0.2. Such small values show that QGP is a strongly-coupled nearly perfect fluid [31, 42]. Contrary to the elliptic flow, the triangular flow is nearly independent of centrality, and can be described using viscous hydrodynamics and transport models too. Triangular flow is a sensitive probe of initial geometry fluctuations and viscosity [43].

The v_2 magnitudes measured at the Super Proton Synchrotron (SPS) energy, $\sqrt{s_{NN}} = 17.3$ GeV, are significantly lower than those measured at the top RHIC and LHC energies. Except for the most central collisions [44], the transverse momentum flow data $v_2(p_T)$ at SPS [45–47], although very similar in shape to the RHIC and LHC data, are below predictions of ideal hydrodynamics [48]. The inability of the ideal hydrodynamics to describe the elliptic flow at the top

SPS energy has been ascribed to insufficient number densities at very early collision stages [49] and strong dissipative effects at the late hadronic stages [31, 32, 50, 51]. The flow measurements have been also performed within the Beam Energy Scan (BES) program at the RHIC from the top incident energy of $\sqrt{s_{NN}} = 200$ GeV down up to the $\sqrt{s_{NN}} = 7.7$ GeV [52, 53]. Also, at the RHIC have been measured various correlations between the Fourier v_n harmonics, among them the ratio v_4/v_2^2 as a function of p_T and centrality [54, 55].

In this paper, we present the first result of negative pions $v_3^{1/3}/v_2^{1/2}$ ratio as a function of transverse momentum in PbAu collisions at the SPS at a nucleon-nucleon center-of-mass energy of $\sqrt{s_{NN}} = 17.3$ GeV. The analysis is based on previously published v_2 and v_3 data [44, 56], where the v_2 data have been rebinned. This reanalysis of the data provides a novel way of highlighting similarities with the flow phenomena seen at RHIC and LHC. The obtained results reveal, independently of the hydrodynamic models, a new interpretation of the SPS data which indicates hydrodynamic behavior of the system formed in PbAu collisions already at top SPS energy. The results are compared with the ATLAS and the ALICE measurements and show a very similar behavior. The results are also compared with predictions from a hybrid model [58] consisting of SMASH (Simulating Many Accelerated Strongly-interacting Handrons) [57], a hadron transport approach suitable for modelling heavy-ion collisions, combined with the vHLLX 3+1D viscous hydrosolver [59] that simulates the QGP expansion, as well as with predictions from the SMASH model applied alone. The paper is organized as follows. Some details concerning the experiment and the data sample are given in Sect. 2. The data analysis and the obtained results are presented in Sect. 3. A short summary is given in Sect. 4.

2 Experiment and data sample

In the year 2000, a sample of $30 \cdot 10^6$ mainly central PbAu events was collected with the upgraded CERES/NA45 spectrometer at the top SPS center-of-mass energy per nucleon pair of $\sqrt{s_{NN}} = 17.3$ GeV. The spectrometer covers the polar angle acceptance of $7.7^\circ \leq \vartheta \leq 14.7^\circ$, corresponding to a pseudorapidity range $2.05 \leq \eta \leq 2.70$ located near midrapidity ($y_{mid} = 2.91$). The CERES/NA45 spectrometer has axial symmetry with respect to the beam direction. As it covers the full 2π azimuthal acceptance, it is very well suited for measurements of the Fourier harmonics of azimuthal distributions. A detailed description of the CERES/NA45 experiment is given in [60].

Momentum determination is provided by the radial-drift Time Projection Chamber (TPC) [61] that is operated inside an axially symmetric magnetic field with a maximum radial

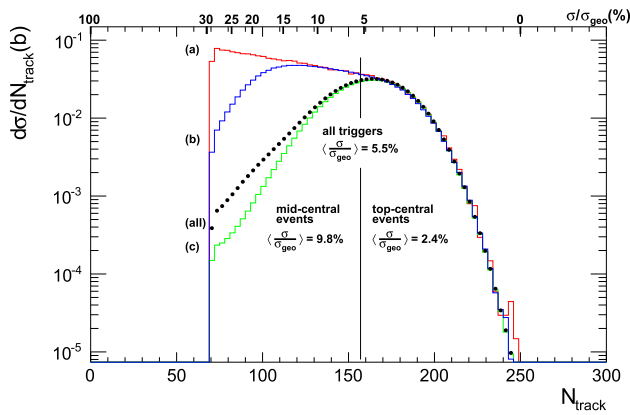


Fig. 1 TPC track density for the trigger mix within (0–30%) centrality. The mix consists of three components: (a) minimum-bias (0.5%), (b) semicentral (8.3%), and (c) central (91.2%), where the parentheses represent the percentage fractions in the mix. The mix of all triggers, with a resulting mean centrality of 5.5%, is labeled as ‘all triggers’ and displayed by closed black circles. The vertical axis gives the differential cross-section expressed in barns (b). The $\langle \sigma / \sigma_{\text{geo}} \rangle$ axis on top gives the fraction of the total inelastic cross section. The figure is taken from Ref. [56]

component of 0.5 T. Negative pions are identified by the differential energy loss dE/dx in the TPC. For vertex reconstruction and tracking outside the magnetic field, two radial silicon drift detectors (SDD) [62] are placed at 10 and 13 cm downstream of a segmented Au target. Negative pions are reconstructed by matching track segments in the SDD doublet and in the TPC. Depending on pion momentum, the relative momentum resolution varies between 2% and 8% for pion momenta of 0.05 to 2.0 GeV/c.

A mix of three triggers designed to enhance central events was used for data collection in the range 0–30% of $\sigma / \sigma_{\text{geo}}$ with an average centrality of 5.5% in the data sample. The multiplicity distribution for all triggers combined (‘all triggers’) is shown in Fig. 1 by the closed black symbols. At low multiplicities, it strongly deviates from the minimum-bias distribution labeled with (a). Beside minimum-bias data, which contribute with only 0.5% of all events, a semi-central trigger, labeled with (b), contributes 8.3% to the total. The biggest share of data, 91.2%, is collected with a most central trigger labeled with (c) in Fig. 1. The results presented in this paper correspond to ‘top-central’ and ‘mid-central’ triggers by selecting $N_{\text{track}} > 159$ and $N_{\text{track}} \leq 159$, with weighted mean centralities of 2.4% and 9.8%, respectively.

3 Analysis and results

The performed analysis uses the event-plane method [63, 64]. The event plane is defined experimentally at high energies by the beam direction and the direction of maximum outgoing particle density, and it is characterized by the event-plane

angle Ψ_n . Each Fourier harmonic order n has its own event plane. The angle Ψ_n is calculated as:

$$\Psi_n = \frac{1}{n} \arctan \frac{\sum_{i=0}^M w_i(p_{Ti}) \sin(n\phi_i)}{\sum_{i=0}^M w_i(p_{Ti}) \cos(n\phi_i)}, \quad n = 2, 3, \quad (1)$$

where ϕ_i is the azimuthal angle of the i th particle out of M particles, with transverse momentum p_{Ti} , used for event-plane reconstruction, and $w_i(p_{Ti})$ are weights used to optimize the event-plane resolution. In order to avoid a trivial autocorrelation effect, and some contribution from short-range correlations, the ϕ coordinate is divided into 100 adjacent equal slices spanning the whole ϕ range. A set made from the each fourth slice forms a ‘sliced subevent’. So, the whole event is divided into 4 sliced subevents each consisting of 25 slices. These four subevents are denoted as a , b , c and d . The n th order event plane is reconstructed by employing tracks that belong to a given sliced subevent. In order to correct for local detector inefficiency, a shifting and flattening procedure is applied (for more details see [65]) to ensure an azimuthally isotropic event-plane distribution. The anisotropy is measured by correlating particles from a given sliced subevent with the event plane obtained from the non-adjacent sliced subevent, i.e. $a - c$ and $b - d$ combinations. The v_n coefficients are then measured with respect to the n^{th} order event plane. The raw v_n coefficients are corrected for the finite event-plane resolution.

The analysis is performed for negative pions.¹ As identical bosons, they are correlated due to the Hanbury Brown and Twiss (HBT) effect [66]. This correlation results in a spurious flow [67]. A standard procedure, that uses the Bertsch-Pratt parametrization described in [67], is applied to suppress the non-flow contribution coming from the HBT effect. Details about the procedure can be found in [44, 56, 65].

The most important source of systematic uncertainty stems from the event plane determination. To contrast to the process analysis, we reduce and estimate this uncertainty by employing two methods. Beside the ‘sliced subevent’ method, the data have been analyzed using the subevent method too. In the subevent method, the event is divided into two subevents, one formed from negative pion, and another one from positive pion candidates selected using a band that corresponds to $\pm 1.5\sigma$ confidence level around the nominal dE/dx energy loss for negative, and for positive pions calculated by using the Bethe-Bloch formula respectively. Again, the autocorrelation effect is removed by correlating the pions from one subevent to the event plane constructed from the other one. The advantage of this approach with respect to the ‘sliced subevent’ method is that the event-plane resolution is better by a factor of about $\sqrt{2}$ due to the twice larger multiplicity used for the event-plane reconstruction [65]. Then,

¹ Using the dE/dx , positive pions could not be well enough separated from protons.

the systematic uncertainty is calculated as an absolute difference between the v_n ($n = 2, 3$) magnitudes calculated from the two methods: the 'sliced subevent' method and the subevent method. At p_T smaller than 0.8 GeV/c, a significant contribution to the systematic uncertainty comes from the correction of the HBT effect too. That part of systematic uncertainty is calculated in the same way as it was done in [44] and in [56]. The maximal absolute systematic uncertainty is about 0.4% at p_T around 0.3 GeV/c, where the HBT effect is largest [56]. For p_T above 0.8 GeV/c, this effect is negligible. The final systematic uncertainty is obtained by summing up in quadrature the uncertainties from the difference between the two methods and the one that comes from the HBT effect. As the uncertainties are uncorrelated, based on the error propagation, the systematic uncertainties for the ratio $v_3^{1/3}/v_2^{1/2}$ are calculated from the corresponding values for the v_2 and v_3 coefficients. The relative systematic uncertainties are large for the ratio $v_3^{1/3}/v_2^{1/2}$, especially for the 'top-central' events class, due to the fact that at lowest p_T the flow magnitudes are close to zero. Corresponding values go from 13% at p_T around 1.0 GeV/c up to about 100% at the lowest p_T bin. Thus, the relative systematic uncertainties of the ratio $v_3^{1/3}/v_2^{1/2}$ dominate over the statistical ones in the low p_T bins and become about 10% in higher p_T bins for the 'top-central' events class. The overall absolute uncertainties are rather tiny.

Figure 2 displays the HBT-corrected v_2 values of negative pions for two centrality classes in PbAu collisions at $\sqrt{s_{NN}} = 17.3$ GeV. The v_2 values of negative pions are taken from [44] and rebinned. In the same figure results from a hybrid model [58] combining the vHLLC viscous hydro-solver [59] with the hadronic transport model SMASH [57] are plotted. The v_n coefficients are calculated using the event-plane method. The centrality ranges for the hydrodynamic calculation are comparable with the experimental ones. The model predictions are calculated for negative pions within $-1 < \eta < 1$ that is close to the experimental acceptance. The value of the specific viscosity used in the vHLLC model is 0.15. For p_T above about 0.6 GeV/c, in both centrality classes the hydrodynamic prediction overestimates the data. The SMASH model data are analyzed using the same event-plane method as in the case of the SMASH-vHLLC model, as well as the same acceptance. In difference to SMASH-vHLLC, the SMASH model alone predicts that v_2 is somewhat below the experimental data for $p_T < 1$ GeV/c. At high p_T , due to the limited statistics in the simulations, v_2 fluctuates a lot.

Figure 3 shows the HBT corrected v_3 values of negative pions for the same two centrality classes in PbAu collisions at $\sqrt{s_{NN}} = 17.3$ GeV. The v_3 values of negative pions are taken from [56]. As in Fig. 2, the results obtained from the above mentioned hybrid model are plotted together with the experimental data. In contrast to the case of the elliptic flow,

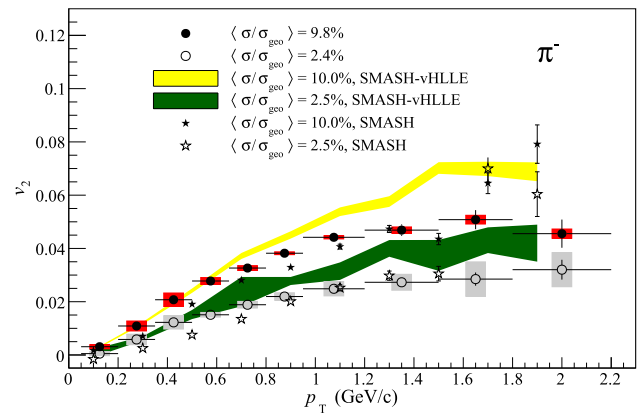


Fig. 2 The transverse momentum dependence of the elliptic flow coefficient, v_2 , for negative pions in PbAu collisions at $\sqrt{s_{NN}} = 17.3$ GeV in two centrality classes. The statistical uncertainties are represented with the vertical bars, while systematic ones are indicated by red and gray rectangles. Also shown are model predictions with their statistical uncertainties as a yellow and green bands (SMASH-vHLLC) and the vertical bars (SMASH)

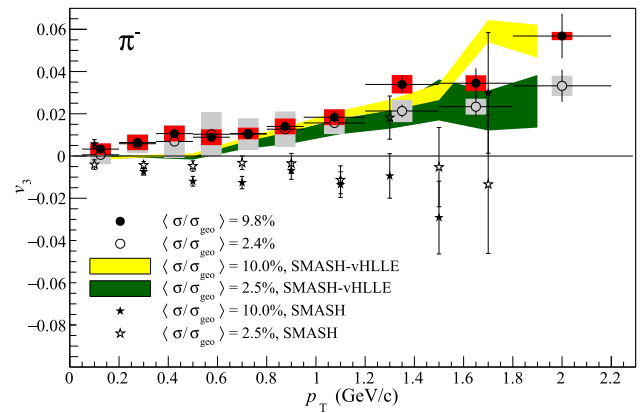


Fig. 3 The transverse momentum dependence of the triangular flow coefficient, v_3 , for negative pions in PbAu collisions at $\sqrt{s_{NN}} = 17.3$ GeV in two centrality classes. The statistical uncertainties are represented with the vertical bars, while systematic ones are indicated by red and gray rectangles. Also shown are model predictions with their statistical uncertainties as a yellow and green bands (SMASH-vHLLC) and the vertical bars (SMASH)

the hydrodynamic calculations are in a good agreement with the data also for p_T above about 0.8 GeV/c. For $p_T < 0.8$ GeV/c, data tend to be above the hydrodynamic prediction for both centrality classes. In difference to the SMASH-vHLLC and the experimental results, the SMASH model alone gives small but negative v_3 that prevents calculation of the ratio $v_3^{1/3}/v_2^{1/2}$. So, a positive v_3 is obtained only in a combination of hydrodynamics vHLLC calculations and the SMASH

² For clarity of the figure, the points for v_3 values for both centrality bins at $p_T = 1.9$ GeV/c are not included in the figure. Their values are -0.158 ± 0.048 and -0.142 ± 0.053 for $\langle \sigma/\sigma_{geo} \rangle = 9.8\%$ and $\langle \sigma/\sigma_{geo} \rangle = 2.4\%$ respectively.

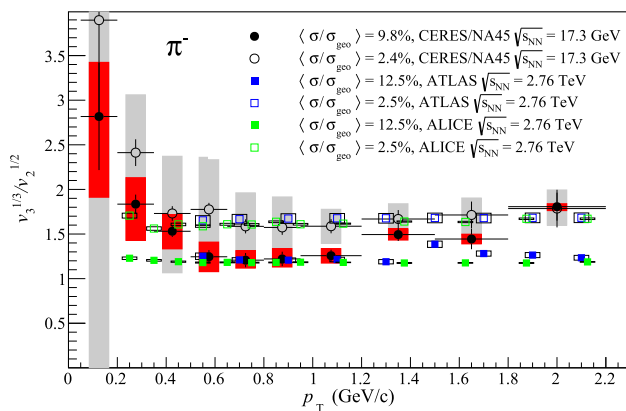


Fig. 4 The ratio $v_3^{1/3}/v_2^{1/2}$ for negative pions as a function of transverse momentum in PbAu collisions at $\sqrt{s_{NN}} = 17.3$ GeV in two centrality classes: ‘top-central’ and ‘mid-central’ events presented with open and closed circles respectively. The statistical uncertainties are represented as the vertical bars, while systematic ones are indicated by red and gray rectangles. The blue and green squares represent corresponding ATLAS [17] and ALICE [69] results. Open boxes represent corresponding systematic uncertainties

model (SMASH-vHLL). A long hydrodynamic evolution of the QGP dominates the collision dynamics.

In the hydrodynamics, at $p_T \lesssim 2$ GeV/c, the $v_n(p_T)$ behave as power-law functions of p_T [43,68]. This can be expressed as

$$v_n(p_T) = c_n p_T^{n/m}, \quad n = 2, 3, \dots, \quad (2)$$

where c_n is a coefficient of proportionality that depends on the order n , and m is a fixed number³ independent of n . In this case, the ratio $v_3^{1/3}/v_2^{1/2}$ becomes a p_T independent number $c_3^{1/3}/c_2^{1/2}$. The ratio depends on centrality. Similar scaling ratios $v_n^{1/n}/v_2^{1/2}$, $n > 2$, as a function of centrality, have been already measured at RHIC [55] and the LHC [17].

Figure 4 shows the ratio $v_3^{1/3}/v_2^{1/2}$ as a function of p_T for two centrality classes. The ratio is calculated for negative pions after suppression of the contribution of the HBT effect to the measured v_n coefficients. The figure also shows the same ratio for PbPb collisions at $\sqrt{s_{NN}} = 2.76$ TeV from the ATLAS [17] and ALICE [69] experiment. The centrality classes are similar to those used by the CERES/NA45 experiment. The ATLAS and ALICE analyses have been performed on charged particles emitted within $|\eta| < 2.5$ and $|\eta| < 0.8$, respectively. There is a very good agreement between the ATLAS (blue squares) and ALICE (green squares) data. Despite the huge difference in incident energies between the top SPS energy and the LHC energy, for p_T above 0.5 GeV/c, the CERES/NA45 data are in a rather good agreement with the ATLAS and ALICE data, especially for the ‘top-central’ events. In the case of ‘mid-central’ events

³ The coefficient c_n and number m can be found from the corresponding fit to the $v_n(p_T)$ distribution.

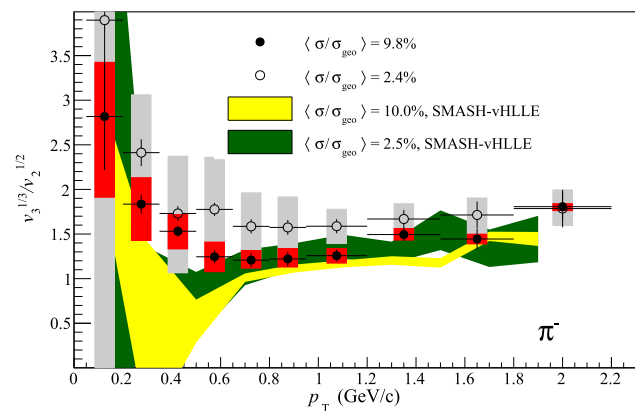


Fig. 5 The ratio $v_3^{1/3}/v_2^{1/2}$ for negative pions as a function of transverse momentum in PbAu collisions at $\sqrt{s_{NN}} = 17.3$ GeV in two centrality classes: ‘top-central’ and ‘mid-central’ events presented with open and closed circles respectively. The statistical uncertainties are represented with the vertical bars, while systematic ones are indicated by red and gray rectangles. Statistical uncertainties are represented with the vertical bars. The statistical uncertainties of the model predictions are shown as a yellow and green band

for $p_T > 1.2$ GeV/c, the CERES/NA45 results are somewhat above the ATLAS and ALICE data. Universally, there is a trend that the ratio for semicentral collisions is smaller. For the present data, there is a rising trend below 500 MeV/c, although not very significant within errors. The uncertainties are significantly larger for the current SPS data due to very small values of $v_{2,3}$ at the lower energy. In the low- p_T range 0.05–0.5 GeV/c, where the HBT influence is largest, it may be that the HBT effect on the measured v_3 harmonic is not completely suppressed, thus producing larger values of the $v_3^{1/3}/v_2^{1/2}$ ratio. A p_T -independent $v_3^{1/3}/v_2^{1/2}$ ratio is a hydrodynamic prediction [43,68]. The CERES/NA45 results imply that the system formed in PbAu collisions at the top SPS energy exhibits hydrodynamic behavior as already suggested in [44].

Figure 5 shows a comparison of the CERES $v_3^{1/3}/v_2^{1/2}$ data with the corresponding ratio calculated by the SMASH-vHLL model. As expected, for $p_T > 0.7$ GeV/c, where the statistical uncertainties of the model are small enough, the model gives a rather flat ratio for both centrality classes. For $p_T < 0.5$ GeV/c, the statistical uncertainties of the model are very large. The SMASH-vHLL model prediction tends to stay slightly below the experimental data. This is due to the fact that the model overestimates the experimentally measured v_2 somewhat for $p_T > 0.7$ GeV/c, while it reproduces v_3 harmonics, as shown in Figs. 2 and 3.

This possibility was already discussed in our first publication of elliptic flow coefficients for pions where data were compared to ideal hydrodynamics calculations [46] as well as in [44]. Then we found that data could be well described using ideal hydrodynamics, and a freeze-out temperature of 160 MeV, while for 120 MeV the flow was over-

predicted for semicentral data. At the time we concluded that a suppression mechanism should be at work not present in ideal hydrodynamic calculations. This is confirmed by the rather good description of the data presented in the current publication with a viscous hydrodynamics calculation. Albeit the comparison presented here is to results of a more recent hydrodynamics code, the suppression is in magnitude entirely consistent with the value of $\eta/s = 0.15$ used here.

These predictions of the hybrid model at SPS tend to be a little below data. In particular, the choice of initial state and η/s value for hydrodynamic evolution is very important. This measurement could help to better constrain the initial conditions and specific viscosity.

4 Summary

The ratio $v_3^{1/3}/v_2^{1/2}$ of negative pions has been measured as a function of p_T using the data collected by the CERES/NA45 experiment for PbAu collisions at $\sqrt{s_{NN}} = 17.3$ GeV. This ratio, measured in two centrality classes, shows rather similar as the LHC results from the ATLAS and ALICE experiments. The SMASH-vHLLLE hybrid model calculations reasonably well represent the data. Only for p_T above about 0.6 GeV/c, the SMASH-vHLLLE hybrid model overestimates the experimentally measured v_2 . The results give a new interpretation of the SPS data at its top energy which indicates hydrodynamic behavior of the system formed in PbAu collisions. These results shed some light on the dynamics of the system created in heavy-ion collisions at top SPS energy. The moderate deviations between data and the current hybrid hydrodynamics calculation could be used in future investigations to fine-tune the initial condition and transport parameters so far rather little explained at SPS energy.

Acknowledgements The CERES/NA45 collaboration acknowledges the good performance of the CERN PS and SPS accelerators as well as the support from the EST division. We are grateful for excellent support by the CERN IT division for the central data recording and data processing. This work was supported by GSI, Darmstadt, the German BMBF, the German VH-VI 146, the US DoE, the Israeli Science Foundation, and the MINERVA Foundation. We acknowledge the support by the Ministry of Education, Science and Technological Development of the Republic of Serbia throughout the theme 0102202. Z.P. acknowledges support by the State of Hesse within the Research Cluster ELEMENTS (Project ID 500/10.006). Computational resources for theoretical modelling have been provided by the GreenCube at GSI. We thank Iurii Karpenko for enlightening discussions with him, and appreciate his help concerning the SMASH-vHLLLE hybrid model.

Funding Ministry of Education, Science and Technological Development (MESTD) has overall responsibility for the research and education system in Serbia.

Data Availability Statement Data will be made available on reasonable request. [Authors' comment: The experimental and model data values obtained during the current study are available from the corresponding author on reasonable request.]

Code Availability Statement Code/software will be made available on reasonable request. [Authors' comment: The code made during the current study is available from the corresponding author on reasonable request.]

Open Access This article is licensed under a Creative Commons Attribution 4.0 International License, which permits use, sharing, adaptation, distribution and reproduction in any medium or format, as long as you give appropriate credit to the original author(s) and the source, provide a link to the Creative Commons licence, and indicate if changes were made. The images or other third party material in this article are included in the article's Creative Commons licence, unless indicated otherwise in a credit line to the material. If material is not included in the article's Creative Commons licence and your intended use is not permitted by statutory regulation or exceeds the permitted use, you will need to obtain permission directly from the copyright holder. To view a copy of this licence, visit <http://creativecommons.org/licenses/by/4.0/>.
Funded by SCOAP³.

References

1. U.W. Heinz, M. Jacob, Evidence for a new state of matter: an assessment of the results from the CERN lead beam program. [arXiv:nucl-th/0002042](https://arxiv.org/abs/nucl-th/0002042)
2. BRAHMS Collaboration, Quark gluon plasma and color glass condensate at RHIC? The perspective from the BRAHMS experiment. *Nucl. Phys. A* **757**, 1 (2005). [arXiv:nucl-ex/0410020](https://arxiv.org/abs/nucl-ex/0410020)
3. PHOBOS Collaboration, The PHOBOS perspective on discoveries at RHIC. *Nucl. Phys. A* **757**, 28 (2005). [arXiv:nucl-ex/0410022](https://arxiv.org/abs/nucl-ex/0410022)
4. STAR Collaboration, Experimental and theoretical challenges in the search for the quark gluon plasma: the STAR Collaboration's critical assessment of the evidence from RHIC collisions. *Nucl. Phys. A* **757**, 102 (2005). [arXiv:nucl-ex/0501009](https://arxiv.org/abs/nucl-ex/0501009)
5. PHENIX Collaboration, Formation of dense partonic matter in relativistic nucleus-nucleus collisions at RHIC: experimental evaluation by the PHENIX collaboration. *Nucl. Phys. A* **757**, 184 (2005). [arXiv:nucl-ex/0410003](https://arxiv.org/abs/nucl-ex/0410003)
6. W. Busza, K. Rajagopal, W. van der Schee, Heavy ion collisions: the big picture, and the big questions. *Ann. Rev. Nucl. Part. Sci.* **68**, 339 (2018). [arXiv:1802.04801](https://arxiv.org/abs/1802.04801) [hep-ph]
7. P. Braun-Munzinger, V. Koch, T. Schäfer, J. Stachel, Properties of hot and dense matter from relativistic heavy ion collisions. *Phys. Rep.* **621**, 76 (2016). [arXiv:1510.00442](https://arxiv.org/abs/1510.00442) [nucl-th]
8. E877 Collaboration, Observation of anisotropic event shapes and transverse flow in Au + Au collisions at AGS energy. *Phys. Rev. Lett.* **73**, 2532 (1994). [arXiv:hep-ex/9405003](https://arxiv.org/abs/hep-ex/9405003)
9. NA49 Collaboration, Stopping and collective effects at SPS energies. *Nucl. Phys. A* **610**, 76 (1996)
10. WA98 Collaboration, Collective flow in 158-A-GeV Pb + Pb collisions. *Nucl. Phys. A* **638**, 459 (1998)
11. CERES Collaboration, Hadron physics with CERES: spectra and collective flow. *Nucl. Phys. A* **638**, 467 (1998)
12. ALICE Collaboration, Elliptic flow of charged particles in Pb-Pb collisions at 2.76 TeV. *Phys. Rev. Lett.* **105**, 252302 (2010). [arXiv:1011.3914](https://arxiv.org/abs/1011.3914) [nucl-ex]
13. ALICE Collaboration, Higher harmonic anisotropic flow measurements of charged particles in Pb-Pb collisions at $\sqrt{s_{NN}}=2.76$ TeV. *Phys. Rev. Lett.* **107**, 032301 (2011). [arXiv:1105.3865](https://arxiv.org/abs/1105.3865) [nucl-ex]

14. ALICE Collaboration, Elliptic flow of identified hadrons in Pb-Pb collisions at $\sqrt{s_{NN}} = 2.76$ TeV. *JHEP* **06**, 190 (2015). [arXiv:1405.4632](#) [nucl-ex]
15. ALICE Collaboration, Anisotropic flow of charged particles in Pb-Pb collisions at $\sqrt{s_{NN}} = 5.02$ TeV. *Phys. Rev. Lett.* **116**, 132302 (2016). [arXiv:1602.01119](#) [nucl-ex]
16. ATLAS Collaboration, Measurement of the pseudorapidity and transverse momentum dependence of the elliptic flow of charged particles in lead-lead collisions at $\sqrt{s_{NN}} = 2.76$ TeV with the ATLAS detector. *Phys. Lett. B* **707**, 330 (2012). [arXiv:1108.6018](#) [hep-ex]
17. ATLAS Collaboration, Measurement of the azimuthal anisotropy for charged particle production in $\sqrt{s_{NN}} = 2.76$ TeV lead-lead collisions with the ATLAS detector. *Phys. Rev. C* **86**, 014907 (2012). [arXiv:1203.3087](#) [hep-ex]
18. ATLAS Collaboration, Measurement of the distributions of event-by-event flow harmonics in lead-lead collisions at $\sqrt{s_{NN}} = 2.76$ TeV with the ATLAS detector at the LHC. *JHEP* **11**, 183 (2013). [arXiv:1305.2942](#) [hep-ex]
19. CMS Collaboration, Centrality dependence of dihadron correlations and azimuthal anisotropy harmonics in PbPb collisions at $\sqrt{s_{NN}} = 2.76$ TeV. *Eur. Phys. J. C* **72**, 2012 (2012). [arXiv:1201.3158](#) [nucl-ex]
20. CMS Collaboration, Measurement of the elliptic anisotropy of charged particles produced in PbPb collisions at $\sqrt{s_{NN}} = 2.76$ TeV. *Phys. Rev. C* **87**, 014902 (2013). [arXiv:1204.1409](#) [nucl-ex]
21. CMS Collaboration, Measurement of higher-order harmonic azimuthal anisotropy in PbPb collisions at $\sqrt{s_{NN}} = 2.76$ TeV. *Phys. Rev. C* **89**, 044906 (2014). [arXiv:1310.8651](#) [nucl-ex]
22. CMS Collaboration, Studies of azimuthal dihadron correlations in ultra-central PbPb collisions at $\sqrt{s_{NN}} = 2.76$ TeV. *JHEP* **02**, 088 (2014). [arXiv:1312.1845](#) [nucl-ex]
23. J.-Y. Ollitrault, Anisotropy as a signature of transverse collective flow. *Phys. Rev. D* **46**, 229 (1992)
24. B. Alver, G. Roland, Collision geometry fluctuations and triangular flow in heavy-ion collisions. *Phys. Rev. C* **81**, 054905 (2010). [arXiv:nucl-th/1003.0194](#). [Erratum: *Phys. Rev. C* **82**, 039903 (2010)]
25. PHOBOS Collaboration, System size, energy, pseudorapidity, and centrality dependence of elliptic flow. *Phys. Rev. Lett.* **98**, 242302 (2007). [arXiv:nucl-ex/0610037](#)
26. PHOBOS Collaboration, Importance of correlations and fluctuations on the initial source eccentricity in high-energy nucleus-nucleus collisions. *Phys. Rev. C* **77**, 014906 (2008). [arXiv:nucl-ex/0711.3724](#)
27. PHENIX Collaboration, Measurements of higher-order flow harmonics in Au+Au collisions at $\sqrt{s_{NN}} = 200$ GeV. *Phys. Rev. Lett.* **107**, 252301 (2011). [arXiv:1105.3928](#) [nucl-ex]
28. X. Sun for the STAR Collaboration, Triangular flow of identified hadrons in Au + Au collisions at $\sqrt{s_{NN}} = 39$ and 200 GeV. *Nucl. Phys. A* **931**, 1194 (2014)
29. S.T.A.R. Collaboration, Beam energy dependence of the third harmonic of azimuthal correlations in Au+Au collisions at RHIC. *Phys. Rev. Lett.* **116**, 112302 (2016). [arXiv:1601.01999](#) [nucl-ex]
30. P. Huovinen, P.V. Ruuskanen, Hydrodynamic models for heavy ion collisions. *Ann. Rev. Nucl. Part. Sci.* **56**, 163 (2006). [arXiv:nucl-th/0605008](#)
31. M. Gyulassy, L. McLerran, New forms of QCD matter discovered at RHIC. *Nucl. Phys. A* **750**, 30 (2005). [arXiv:nucl-th/0405013](#)
32. T. Hirano, U. Heinz, D. Kharzeev, R. Lacey, Y. Nara, Hadronic dissipative effects on elliptic flow in ultrarelativistic heavy-ion collisions. *Phys. Lett. B* **636**, 299 (2006). [arXiv:nucl-th/0511046](#)
33. T. Hirano, P. Huovinen, Y. Nara, Elliptic flow in U+U collisions at $\sqrt{s_{NN}} = 200$ GeV and in Pb+Pb collisions at $\sqrt{s_{NN}} = 2.76$ TeV: Prediction from a hybrid approach. *Phys. Rev. C* **83**, 021902 (2011). [arXiv:1010.6222](#) [nucl-th]
34. D. Teaney, J. Lauret, E.V. Shuryak, Hydro+cascade, flow, the equation of state, predictions and data. *Nucl. Phys. A* **698**, 479 (2002). [arXiv:nucl-th/0104041](#)
35. P. Romatschke, U. Romatschke, Viscosity information from relativistic nuclear collisions: how perfect is the fluid observed at RHIC? *Phys. Rev. Lett.* **99**, 172301 (2007). [arXiv:0706.1522](#) [nucl-th]
36. B. Schenke, S. Jeon, C. Gale, (3+1)D hydrodynamic simulation of relativistic heavy-ion collisions. *Phys. Rev. C* **82**, 014903 (2010). [arXiv:1004.1408](#) [hep-ph]
37. B. Schenke, S. Jeon, C. Gale, Elliptic and triangular flow in event-by-event (3+1)D viscous hydrodynamics. *Phys. Rev. Lett.* **106**, 042301 (2011). [arXiv:1009.3244](#) [hep-ph]
38. C. Shen, Z. Qiu, H. Song, J. Bernhard, S. Bass, U. Heinz, The iEBE-VISHNU code package for relativistic heavy-ion collisions. *Comput. Phys. Commun.* **199**, 61 (2016). [arXiv:1409.8164](#) [nucl-th]
39. C. Gale, S. Jeon, B. Schenke, P. Tribedy, R. Venugopalan, Event-by-event anisotropic flow in heavy-ion collisions from combined Yang-Mills and viscous fluid dynamics. *Phys. Rev. Lett.* **1**, 012302 (2013). [arXiv:1209.6330](#) [nucl-th]
40. H. Song, S. Bass, U. Heinz, T. Hirano, C. Shen, Hadron spectra and elliptic flow for 200 A GeV Au+Au collisions from viscous hydrodynamics coupled to a Boltzmann cascade. *Phys. Rev. C* **83**, 054910 (2011). [arXiv:1101.4638](#) [nucl-th]
41. J.E. Bernhard, J.S. Moreland, S.A. Bass, Bayesian estimation of the specific shear and bulk viscosity of quark-gluon plasma. *Nat. Phys.* **15**, 1113 (2019)
42. E. Shuryak, A strongly coupled quark-gluon plasma. *J. Phys. G* **30**, S1221 (2004)
43. B. Alver, C. Gombeaud, M. Luzum, J.-Y. Ollitrault, Triangular flow in hydrodynamics and transport theory. *Phys. Rev. C* **82**, 034913 (2010). [arXiv:1007.5469](#) [nucl-th]
44. NA45/CERES Collaboration, Elliptic flow of charged pions, protons and strange particles emitted in Pb+Au collisions at top SPS energy. *Nucl. Phys. A* **894**, 41 (2012). [arXiv:1205.3692](#) [nucl-ex]
45. NA49 Collaboration, Directed and elliptic flow of charged pions and protons in Pb + Pb collisions at 40-A-GeV and 158-A-GeV. *Phys. Rev. C* **68**, 034903 (2003). [arXiv:nucl-ex/0303001](#)
46. NA45/CERES Collaboration, Semihard scattering unraveled from collective dynamics by two pion correlations in 158-A-GeV / c Pb + Au collisions. *Phys. Rev. Lett.* **92**, 032301 (2004). [arXiv:nucl-ex/0303014](#)
47. WA98 Collaboration, Centrality and transverse momentum dependence of collective flow in 158-A-GeV Pb+Pb collisions measured via inclusive photons. *Nucl. Phys. A* **762**, 129 (2005). [arXiv:nucl-ex/0410045](#)
48. P. Huovinen, P.F. Kolb, U. Heinz, P.V. Ruuskanen, S.A. Voloshin, Radial and elliptic flow at RHIC: further predictions. *Phys. Lett. B* **503**, 58 (2001). [arXiv:hep-ph/0101136](#)
49. U. Heinz, P. Kolb, Rapidity dependent momentum anisotropy at RHIC. *J. Phys. G* **30**, S1229 (2004). [arXiv:nucl-th/0403044](#)
50. D. Teaney, The effects of viscosity on spectra, elliptic flow, and HBT radii. *Phys. Rev. C* **68**, 034913 (2003). [arXiv:nucl-th/0301099](#)
51. H. Niemi, G.S. Denicol, P. Huovinen, E. Molnar, D.H. Rischke, Influence of the shear viscosity of the quark-gluon plasma on elliptic flow in ultrarelativistic heavy-ion collisions. *Phys. Rev. Lett.* **106**, 212302 (2011). [arXiv:1101.2442](#) [nucl-th]
52. STAR Collaboration, Measurement of elliptic flow of light nuclei at $\sqrt{s_{NN}} = 200, 62.4, 39, 27, 19.6, 11.5,$ and 7.7 GeV at the BNL Relativistic Heavy Ion Collider. *Phys. Rev. C* **94**, 034908 (2016). [arXiv:1601.07052](#) [nucl-ex]
53. STAR Collaboration, Centrality dependence of identified particle elliptic flow in relativistic heavy ion collisions at $\sqrt{s_{NN}} = 7.7-6.24$ GeV. *Phys. Rev. C* **93**, 014907 (2016). [arXiv:1509.08397](#) [nucl-ex]

54. STAR Collaboration, Azimuthal anisotropy in Au+Au collisions at $\sqrt{s_{NN}} = 200$ GeV. *Phys. Rev. C* **72**, 01490 (2005). [arXiv:nucl-ex/0409033](#)
55. PHENIX Collaboration, Elliptic and hexadecapole flow of charged hadrons in Au+Au collisions at $\sqrt{s_{NN}} = 200$ GeV. *Phys. Rev. Lett.* **105**, 062301 (2010). [arXiv:1003.5586](#) [nucl-ex]
56. NA45/CERES Collaboration, Triangular flow of negative pions emitted in PbAu collisions at $\sqrt{s_{NN}} = 1.73$ GeV. *Nucl. Phys. A* **957**, 99 (2017). [arXiv:1604.07469](#) [nucl-ex]
57. SMASH Collaboration, J. Weil et al., Particle production and equilibrium properties within a new hadron transport approach for heavy-ion collisions. *Phys. Rev. C* **94**, 054905 (2016). [arXiv:1606.06642](#) [nucl-th]
58. A. Schäfer, I. Karpenko, X.-Y. Wu, J. Hammelmann, H. Elfner, Particle production in a hybrid approach for a beam energy scan of Au+Au/Pb+Pb collisions between $\sqrt{s_{NN}} = 4.3$ GeV and $\sqrt{s_{NN}} = 200.0$ GeV. *Eur. Phys. J. A* **58**, 230 (2022). [arXiv:2112.08724](#) [hep-ph]
59. I. Karpenko, P. Huovinen, M. Bleicher, A 3+1 dimensional viscous hydrodynamic code for relativistic heavy ion collisions. *Comput. Phys. Commun.* **185**, 3016 (2014). [arXiv:1312.4160](#) [nucl-th]
60. NA45/CERES Collaboration, New results from CERES. *J. Phys. G* **30**, S709 (2004). [arXiv:nucl-ex/0406007](#)
61. NA45/CERES Collaboration, The CERES/NA45 radial drift time projection chamber. *Nucl. Instr. Methods A* **593**, 203 (2008). [arXiv:0802.1443](#) [nucl-ex]
62. P. Holl, P. Rehak, F. Ceretto, U. Faschingbauer, J.P. Wurm, A. Castoldi, E. Gatti, A 55 cm^2 cylindrical silicon drift detector. *Nucl. Instr. Methods A* **377**, 367 (1996)
63. S. Voloshin, Y. Zhang, Flow study in relativistic nuclear collisions by Fourier expansion of Azimuthal particle distributions. *Z. Phys. C* **70**, 665 (1994)
64. A.M. Poskanzer, S.A. Voloshin, Methods for analyzing anisotropic flow in relativistic nuclear collisions. *Phys. Rev. C* **58**, 1671 (1998). [arXiv:nucl-ex/9805001](#)
65. J. Milosevic, Investigation of Azimuthal Asymmetries in Charged and Strange Particle Distributions from CERES, Doctoral Thesis, Universität Heidelberg (2006)
66. R. Hanbury Brown, R.Q. Twiss, A New type of interferometer for use in radio astronomy. *Philos. Mag. Ser.* **45**, 663 (1954)
67. P.M. Dinh, N. Borghini, J.-Y. Ollitrault, Effects of HBT correlations on flow measurements. *Phys. Lett. B* **477**, 51 (2000). [arXiv:nucl-th/9912013](#)
68. N. Borghini, J.-Y. Ollitrault, Momentum spectra, anisotropic flow, and ideal fluids. *Phys. Lett. B* **642**, 227 (2006). [arXiv:nucl-th/0506045](#)
69. ALICE Collaboration, Energy dependence and fluctuations of anisotropic flow in Pb-Pb collisions at $\sqrt{s_{NN}} = 5.02$ and 2.76 TeV. *JHEP* **07**, 103 (2018). [arXiv:1804.02944](#) [nucl-ex]